Human-Humanoid Collaborative Carrying

Don Joven Agravante, Andrea Cherubini, Alexander Sherikov, Pierre-Brice Wieber, Abderrahmane Kheddar

▶ **To cite this version:**

Don Joven Agravante, Andrea Cherubini, Alexander Sherikov, Pierre-Brice Wieber, Abderrahmane Kheddar. Human-Humanoid Collaborative Carrying. 2016. lirmm-01311154v2

HAL Id: lirmm-01311154

https://hal-lirmm.ccsd.cnrs.fr/lirmm-01311154v2

Preprint submitted on 27 Nov 2017 (v2), last revised 10 Apr 2019 (v3)

HAL is a multi-disciplinary open access archive for the deposit and dissemination of scientific research documents, whether they are published or not. The documents may come from teaching and research institutions in France or abroad, or from public or private research centers.

L'archive ouverte pluridisciplinaire **HAL**, est destinée au dépôt et à la diffusion de documents scientifiques de niveau recherche, publiés ou non, émanant des établissements d'enseignement et de recherche français ou étrangers, des laboratoires publics ou privés.

Human-Humanoid Collaborative Carrying

Don Joven Agravante[1], Andrea Cherubini[1], Alexander Sherikov[2],
Pierre-Brice Wieber[2] and Abderrahmane Kheddar[1,3],

***Abstract*—This paper contributes to the field of human-robot interaction, specifically physical human-robot collaboration. We present a complete control framework which aims at making humanoid robots capable of carrying objects together with humans. Firstly, we design a template identifying the primitive subtasks necessary for collaborative carrying. Then, these subtasks are formulated as constrained optimization problems for controlling the whole-body motion of a humanoid robot. The subtasks include two walking pattern generators that account for physical collaboration, as well as posture and grasping controllers. Finally, we validate our framework in a variety of collaborative carrying experiments, using the HRP-4 humanoid robot.**

***Index Terms*—Physical Human-Robot Interaction.**

I. Introduction

PHYSICAL human-robot collaboration implies that the interaction forces between the human and robot must be used to achieve a common goal. In this regard, humanoid robots provide many advantages when working together with humans to perform various tasks. Humans learn to physically collaborate with one another from daily experiences. Therefore, a humanoid with a similar range of motion and sensing has the potential to be an intuitive interface. Within physical collaboration, carrying objects with a human in various postures and situations is a problem that is rich, unexplored and has high potential for practical application.

Early work on enabling human-humanoid carrying was done in [1] via the Humanoid Robotics Project (HRP), where the HRP-2P humanoid cooperates with a human for a panel transportation task. Disregarding the legged aspect, even earlier work in this topic was done in [2]. The authors used *mobile manipulator* robots as in [3], with wheels instead of legs. That work revealed an important issue: coordinating the motion of the mobile base with that of the upper robot body and with the human intention (generally represented by the interaction force). More recent examples of collaborative carrying mobile manipulators include [4], [5], [6]. Although these works discuss the handling of interaction forces and coordination, the topic of balance is missing.

This work was partially supported by the EU H2020 COMANOID (www.comanoid.com) project and by the bpifrance PSPC ROMEO 2 (www.projetromeo.com) national project.

[1]CNRS-University of Montpellier, LIRMM, Interactive Digital Human Group, Montpellier, France.

[2]Inria Rhône-Alpes, BIPOP Team, Montbonnot, France.

[3]CNRS-AIST Joint Robotics Laboratory (JRL), Tsukuba, Japan.

This paper has supplementary video downloadable material available at http://ieeexplore.ieee.org.

Color versions of one or more of the figures in this paper are available online at http://ieeexplore.ieee.org.

Digital Object Identifier 00.0000/TRO.201X.0000000

However, as discussed in [7], [8], even wheeled robots can fall over in challenging scenarios. One of the main contributions of this paper is to tackle the coupling of balanced legged locomotion and collaborative manipulation.

The task of collaborative carrying has also been tested on small scale humanoid platforms, e.g., NAO in [9]. However [9] focused on the use of internal sensors, instead of the wrist force/torque sensors commonly used in physical human-robot interaction. NAO is also used in [10], where the capture point [11], [12] guides walking. A similar work is [13], where Darwin robots carry a stretcher (no human is participating). When only robots are used (e.g. simulated HRP-2 robots in [14]), the interest is turned to multi-robot synchronization and communication. Both multi-robot and human aspects are considered in [15], while [16] addresses table lifting with NAO, using machine learning to improve interaction.

Understanding and improving physical human-robot interaction is a very broad and active research field. For example, [17], [18], [19] study human-human haptic interaction and apply it to human-robot teams. Role allocation and role switching (e.g., between leader and follower) have been studied in [20], [21], [22], [23]. The authors of [24] address mutual learning and adaptation, whereas [25] focuses on the uncertainty of human behavior prediction. Haptic interaction recognition using supervised learning is presented in [26].

Contrary to these, this paper presents the entire pipeline required by a humanoid to realize collaborative carrying. Specifically, we embed a humanoid robot with a control framework that allows it to achieve a large variety of human-humanoid carrying tasks.

Our previous framework, specific to table carrying [27], could not be extended to any posture (and therefore objects), since the used walking pattern generator (WPG) [28] and Stack-of-Tasks whole-body controller [29] considered the center of mass (CoM) to be coincident with the robot waist. Hence, any posture moving the CoM away from the waist (e.g. extending the arms or leaning with the chest) would fail. More generally, the WPG of [28] worked well for standalone walking, but was not designed for physical interaction, as explained in [30].

Given these limitations, we reformulate the entire pipeline to have a generic framework for humanoid collaborative carrying. The contributions of this paper follow.

- Two pattern generators for *walking under sustained forces* are designed, one for a leader and the other for a follower robot. Although these were outlined in [30], further details on the modeling choices and on the integration

0000–0000/00$00.00 © 201X IEEE

with whole-body control are given here. Furthermore, we discuss the WPG trajectory feasibility and analyze the underlying model predictive control problem.
- Our whole-body framework can simultaneously *account for both the carrying tasks and walking*. We show how collaborative carrying can be formulated as an optimization problem, and provide details on its feasibility.
- The framework feasibility is validated in a series of experiments on a *real-size humanoid robot*, with a variety of robot roles (leader/follower), grasp types (hand/body) and carried objects (different shapes and sizes).

We structured the paper as follows. Section II presents the collaborative carrying taxonomy, along with the required primitive subtasks. Section III provides a review of quadratic optimization which is used throughout our work. The walking pattern generators accounting for physical interaction are presented in Section IV. Section V describes our optimization framework for whole-body control. Finally, Section VI presents the experimental validation.

II. The Task of Collaborative Carrying

To understand collaborative carrying, we take inspiration from how humans do it. This is done by creating a taxonomy, i.e., an abstraction layer that provides a scaffold for our quadratic optimization framework. Then, we design a Finite State Machine (FSM) accounting for all collaborative carrying subtasks in order to map each state to an optimization problem.

A. A taxonomy of collaborative carrying

We consider the problem of *having a pair of agents, whose goal is to move a specified object from one location to another*. Figure 1 shows several real examples of human-human collaborative carrying (left), with the corresponding simulations of what we envision with a humanoid robot collaborator (right). We assume that neither object nor agent composition can be changed afterwards, and consider the following relationships:

- Agent-object relation (*grasp type*). We consider two broad classes of grasp types: *hand grasps* and *body grasps*. *Hand grasps* are those with contact points located uniquely on the hand/gripper [31]. *Body grasps* are those that utilize grasp contacts on body parts not limited to the hand (e.g., arms, torso, see Fig. 1).
- Agent-agent relation (*relative pose*). In our taxonomy, we relate this to the inter-agent communication modes, touch and vision. For translations, we check whether direct touch between the agents is possible (*near* relation) or not (*far*). For the orientation, we consider the agents' Field Of View (FOV), specifically: the nominal (when the perceiving agent is in a resting position), and the extended (as the agent looks around, by moving its body) FOV. Then, we can classify agents as facing *front* (other agent is in the nominal FOV), *side* (other agent is not in the nominal but in the extended FOV), *back* (other agent is not in the extended FOV).

Fig. 1. Collaborative carrying examples (left), with a human avatar and a humanoid robot mimicking the corresponding postures (right).

All six scenarios of Fig. 1 can be easily classified according to the proposed taxonomy. But more importantly, we are concerned with the practical implications of using the taxonomy to program a humanoid robot.

B. Collaborative carrying as a Finite State Machine

To program a robot for collaborative carrying, we must decompose complex tasks into subtasks that will be easier to program. Formally, we use an FSM to describe the whole task, with subtasks as states. The FSM should be general enough for all cases encompassed by the taxonomy. Although we will create a specific FSM, the use of FSMs is common (e.g., it was applied for humanoid ladder climbing in [32]).

A useful decomposition is one where the states can be easily mapped to optimization problems. We first consider the state transitions. These should include brief periods where the motion is minimal, and the robot can be considered in *quasi-static* state (i.e., dynamic effects can be disregarded), as well as discrete changes in the robot contact state. The state transitions can be triggered either by relevant sensed variables (when available), or by human input (in case of shared autonomy). Considering this, a collaborative carrying FSM is shown in Fig. 2 (the numbers indicate the transition order).

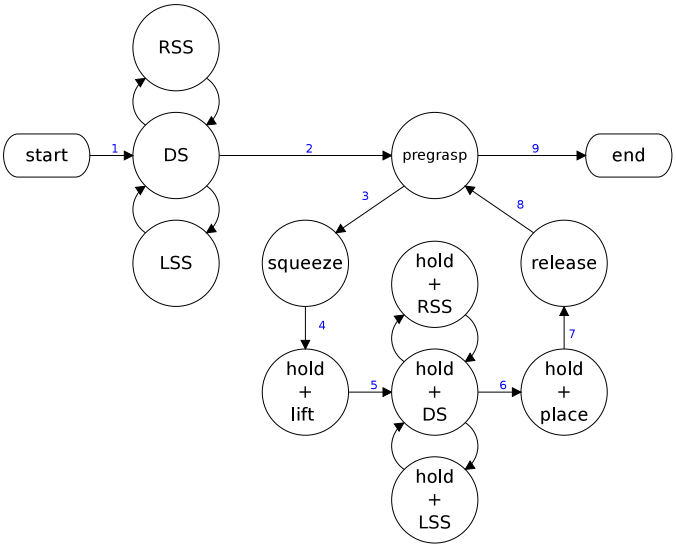

Fig. 2. Detailed FSM for collaborative carrying, with each state/subtask corresponding to an optimization problem.

While walking, the feet contacts occur in a predictable pattern that can be used to define the walking states: left/right single support, and double support (indicated respectively as LSS/RSS and DS in Fig. 2). To decompose grasping, we need a *pregrasp* posture, i.e., a waypoint between grasping and the other states. The next state, *squeeze*, moves the robot to generate predefined contacts between its body and the object. Figure 3 shows the pregrasp and squeezing postures for two body grasps. The *hold* state maintains the contacts between robot and object. Note that it must be active throughout the carrying walk. Finally, the *release* state, is simply the inverse of *squeeze*. Force or tactile sensors, when available, can trigger transitions between these states.

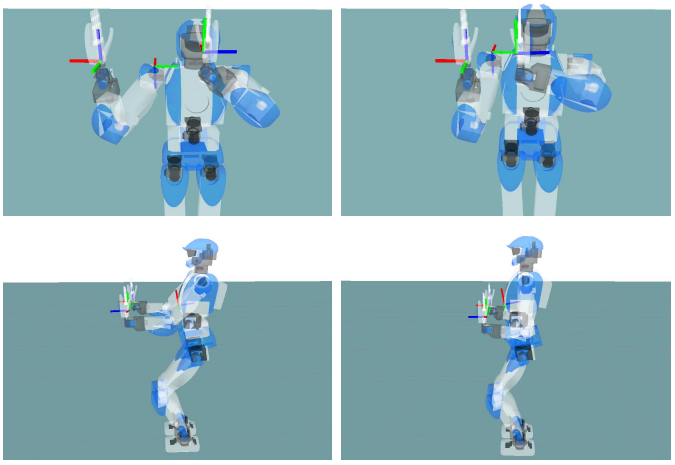

Fig. 3. Two examples of "body grasps": pregrasp (left) and squeeze (right).

In summary, we assign specific optimization problems to each state of the FSM in Fig. 2. The next Section III outlines the general optimization formulation that has been used for all states. This formulation is utilized for generating walks accounting for external force (Section IV), as well as for whole body control (WBC), see Section V. Figure 4 shows how the various parts of the framework fit together, and which section of the paper details which part.

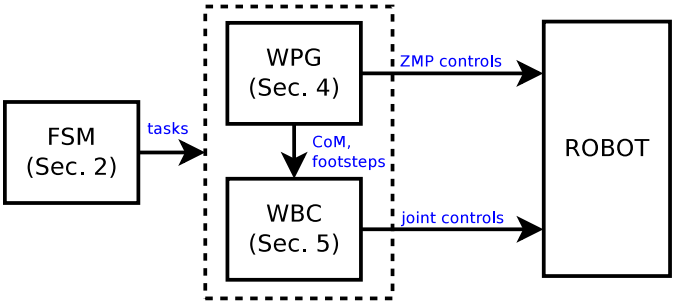

Fig. 4. Simple block diagram of the overall framework

III. Introduction to Quadratic Optimization

Recently, optimization-based approaches have shown to be very effective for controlling humanoid robots. This is true for both WPG [28] and WBC [29], [32], [33], [34], [35], [36].

In general, we seek the robot control input, represented by the optimization argument $\mathbf{x}$ that minimizes a collection of objective functions, subject to various constraints (from the robot hardware, environment, and task).

The formalism chosen here is largely based on [32], [37]. We consider a *weighted quadratic programming* formulation which allows to use the L^2 norm to define a number of objective functions $f_i(\mathbf{x})$:

$$f_i(\mathbf{x}) = \|\mathbf{A}_i\mathbf{x} - \mathbf{b}_i\|^2 , \quad (1)$$

so that all optimization problems are of the form:

$$\underset{\mathbf{x}}{\text{argmin}} \quad \sum_i w_i \left\|\mathbf{A}_i\mathbf{x} - \mathbf{b}_i\right\|^2 \tag{2a}$$

$$\text{subject to} \quad \mathbf{A}_c\mathbf{x} \leq \mathbf{b}_c. \tag{2b}$$

The control input $\mathbf{x}$ is defined via the objectives (2a), which are regarded in accordance to their scalar weights $w_i > 0$. Equality and inequality constraints (2b) must also be satisfied. When this is not possible, the optimization problem is *infeasible* and the constraints are said to be in *conflict*. Infeasibility can be accounted for, by relaxing the conflicting constraints as is common in *hierarchical optimization* [38], or as explained later in the paper for individual optimization problems. Formulation (2) allows the use of off-the-shelf Quadratic Programming (QP) solvers implementing efficient algorithms and suitable for real-time applications [39].

IV. Walking designed for physical collaboration

In robotics, walking has historically been treated separately from manipulation. However, manipulation and locomotion must be consistent, in particular during collaborative carrying. Eventually, both need to be thought of as parts of the whole-body control problem (discussed in the next section). In this section, we revisit the modeling of walking pattern generators (WPG), and redesign them with physical collaboration in mind. This section was partially published in [30]. Here, we recall the main points, namely the addition of the external wrench into the model, and the design of objectives and constraints, based on this wrench. Additionally, we better specify the usage of our new WPG in the collaborative carrying task.

A. Modeling

First, we must design a reduced robot dynamic model accounting for physical interaction. Three possible versions of such models were proposed in [40]:

1) a model with full knowledge of object and/or human,
2) a model that considers the effects of the object and/or human on the robot contact locations and linear forces, requiring additional grasp stability constraints,
3) a model that considers the effects of the object and/or human as external wrenches applied on the robot CoM.

We have chosen the latter, because of its simplicity and generality in terms of implementation on a real robot.

The development of this reduced model is inspired by [41], and described in [30]. We separate the foot/ground contact forces from other interaction contact forces that are denoted by $\mathbf{h}_{\text{ext}} = [\mathbf{f}_{\text{ext}}^\top \ \mathbf{n}_{\text{ext}}^\top]^\top \in \mathbb{R}^6$. This represents the *external wrench* (from the carried object weight and from the human collaborator), and is expressed in a fixed orientation frame placed on the Center of Mass (CoM), $\mathbf{c}$. As is common in the literature [28], [42], we aim at keeping the center of pressure $\mathbf{z}$ (also known as Zero Moment Point, ZMP) within the support polygon (i.e., the convex hull of the feet contact points). We assume that the robot is walking on a flat horizontal ground, with a constant CoM height c^{z}, and that the angular momentum is constant. Then, Newton and Euler equations yield the following relationship between CoM and ZMP:

$$\begin{aligned}\mathbf{z}^{\text{x,y}} = \mathbf{c}^{\text{x,y}} &- \left(\frac{c^{\text{z}}}{g^{\text{z}} - \frac{f^{\text{z}}_{\text{ext}}}{m}}\right)\ddot{\mathbf{c}}^{\text{x,y}} \\ &+ \begin{bmatrix} 0 & 1 \\ -1 & 0 \end{bmatrix}\left(\frac{\mathbf{n}^{\text{x,y}}_{\text{ext}}}{mg^{\text{z}} - f^{\text{z}}_{\text{ext}}}\right) + \left(\frac{c^{\text{z}}\mathbf{f}^{\text{x,y}}_{\text{ext}}}{mg^{\text{z}} - f^{\text{z}}_{\text{ext}}}\right),\end{aligned} \tag{3}$$

with m the robot mass and $\mathbf{g}$ the gravity vector. In the absence of an external wrench, this becomes:

$$\mathbf{z}^{\text{x,y}} = \mathbf{c}^{\text{x,y}} - \left(\frac{c^{\text{z}}}{g^{\text{z}}}\right)\ddot{\mathbf{c}}^{\text{x,y}}, \tag{4}$$

From (3), we can infer that a heavier robot, lower CoM height or an external force aligned with the CoM, will all reduce the effects of the external wrench.

B. Model predictive control for walking

Model Predictive Control (MPC) consists in controlling a system so that future states are taken into account. A common MPC methodology consists in iteratively applying the model over N discrete steps (noted $k = 1 \dots N$), resulting in a new problem formulation where the predicted states are a function of the current state and of the current and future control inputs.

We assume that the CoM trajectory is differentiable three times, so that the walk can be controlled through the CoM jerk. Then, to apply MPC, we define:

- the control input $\mathbf{x} = [\tilde{\mathbf{u}}\ \tilde{\mathbf{r}}]^\top$, with $\tilde{\mathbf{u}}$ and $\tilde{\mathbf{r}}$ the concatenation, over the preview horizon, respectively of the CoM jerk $[\dddot{c}^x_k\ \dddot{c}^y_k]$ and of future foot landing positions, expressed in a *local frame* placed at the preceding foot;
- the system state $\tilde{\mathbf{c}}$ as the concatenation of CoM position, velocity and acceleration $[c^x_k\ \dot{c}^x_k\ \ddot{c}^x_k\ c^y_k\ \dot{c}^y_k\ \ddot{c}^y_k\ ]^\top$;
- the system output $\tilde{\mathbf{z}}$ as the concatenation of $[z^x_k\ z^y_k]^\top$, expressed in the current foot frame;
- the predicted external wrench $\tilde{\mathbf{f}}$ as the concatenation of $[n^y_k\ f^x_k\ n^x_k\ f^y_k]^\top$, considered a perturbation or part of the control input, depending on the WPG design (see below).

Then, propagating (3) over the preview horizon yields:

$$\begin{aligned}\tilde{\mathbf{c}} &= \mathbf{S}\mathbf{x} + \mathbf{s}, \\ \tilde{\mathbf{z}} &= \mathbf{S}_{\text{z}}\mathbf{x} + \mathbf{s}_{\text{z}},\end{aligned} \tag{5}$$

with matrices $\mathbf{S}$, $\mathbf{S}_{\text{z}}$, vectors $\mathbf{s}$, $\mathbf{s}_{\text{z}}$ derived from the current state and from $\tilde{\mathbf{f}}$, as detailed in [30].

As argument of the optimization problem (2) we use $\mathbf{x}$. Then, the objectives and constraints common to all of our WPG formulations are listed below.

- The CoM jerk is minimized to smoothen the trajectory. This is done via objective function:

$$\left\|\tilde{\mathbf{u}}\right\|^2 = \left\|\begin{bmatrix}\mathbf{I} & \mathbf{0}\end{bmatrix}\mathbf{x}\right\|^2. \tag{6}$$

- The distance between ZMP and foot center is minimized to increase the stability margin (since unknown disturbances could push the ZMP away from the target):

$$\left\|\tilde{\mathbf{z}}\right\|^2 = \left\|\mathbf{S}_{\text{z}}\mathbf{x} + \mathbf{s}_{\text{z}}\right\|^2. \tag{7}$$

- The ZMP should be maintained within the support polygon (with security margins) using the constraint[1]:

$$\underline{\tilde{\mathbf{z}}} \leq \tilde{\mathbf{z}} \leq \overline{\tilde{\mathbf{z}}}. \tag{8}$$

Using (5) to expose the argument:

$$\underline{\tilde{\mathbf{z}}} - \mathbf{s}_z \leq \mathbf{S}_z\mathbf{x} \leq \overline{\tilde{\mathbf{z}}} - \mathbf{s}_z. \tag{9}$$

- The feet positions should be constrained:

$$\underline{\tilde{\mathbf{r}}} \leq \tilde{\mathbf{r}} \leq \overline{\tilde{\mathbf{r}}}. \tag{10}$$

Since $\tilde{\mathbf{r}}$ is part of the argument, this can be written as:

$$\underline{\tilde{\mathbf{r}}} \leq \begin{bmatrix}\mathbf{0} & \mathbf{I}\end{bmatrix}\mathbf{x} \leq \overline{\tilde{\mathbf{r}}}. \tag{11}$$

Note that objectives (6), (7) are expressed as (1), and constraints (9), (11) as (2b).

Using (5), we can now design various WPG, suited to different types of physical interaction. In particular, we revisit the *leader* and *follower* modalities [22]. Apart from the common constraints and objectives cited above, the leader and follower WPG are each characterized by a specific formulation of the objective function controlling the CoM.

1) Walking pattern generator for a follower robot:
A follower robot acts based on the leader's intention. In our work, this is represented by the external wrench applied by the carrying partner. Usually, moving the object together implies only a planar motion such that the intention can be defined by $\mathbf{f}_{\text{ext}}^{\text{x,y}}$. Hence, a follower WPG depends on these. Previous works [22], [27] have used a damping control by providing a reference CoM velocity to the WPG which is proportional to the external force. We extend this to perform more complex behaviors, by defining the full impedance model [43] of the follower, with diagonal matrices $\mathbf{M}$, $\mathbf{B}$ and $\mathbf{K}$ containing the virtual mass, damping and stiffness parameters:

$$\mathbf{f}_{\text{ext}}^{\text{x,y}} = \mathbf{M}\ddot{\mathbf{c}}^{x,y} + \mathbf{B}\dot{\mathbf{c}}^{x,y} + \mathbf{K}\mathbf{c}^{x,y}. \tag{12}$$

Using an impedance parameter matrix $\mathbf{G}_{\text{mbk}}$ and a selection matrix $\mathbf{S}_{\text{f}}$ (for choosing either $f_{\text{ext}}^{\text{x}}$ or $f_{\text{ext}}^{\text{y}}$), this expression can be propagated, so that the MPC will aim at minimizing:

$$\left\|\mathbf{G}_{\text{mbk}}\tilde{\mathbf{c}} - \mathbf{S}_{\text{f}}\tilde{\mathbf{f}}\right\|^2 = \left\|\mathbf{G}_{\text{mbk}}\mathbf{S}\mathbf{x} + \mathbf{G}_{\text{mbk}}\mathbf{s} - \mathbf{S}_{\text{f}}\tilde{\mathbf{f}}\right\|^2. \tag{13}$$

Note that by injecting (5), we have expressed this objective as (1). The optimization problem, including objectives (6), (7), (13), and constraints (8), (10) is:

$$\begin{aligned}\underset{\mathbf{x}}{\text{argmin}} \quad & w_{\text{com}}\left\|\tilde{\mathbf{u}}\right\|^2 + w_{\text{zmp}}\left\|\tilde{\mathbf{z}}\right\|^2 + w_{\text{fol}}\left\|\mathbf{G}_{\text{mbk}}\tilde{\mathbf{c}} - \mathbf{S}_{\text{f}}\tilde{\mathbf{f}}\right\|^2 \\ \text{subject to} \quad & \underline{\tilde{\mathbf{z}}} \leq \tilde{\mathbf{z}} \leq \overline{\tilde{\mathbf{z}}} \\ & \underline{\tilde{\mathbf{r}}} \leq \tilde{\mathbf{r}} \leq \overline{\tilde{\mathbf{r}}}.\end{aligned} \tag{14}$$

Notice that the future wrench values are required in $\tilde{\mathbf{f}}$, to make the robot *proactive*. Having a good model of human intention can be difficult, but if the force can be measured (e.g. by a force/torque sensor) at each iteration, we can use a simplistic model $\mathbf{f}_{\text{N}} = ... = \mathbf{f}_1 = \mathbf{f}_0$, with $\mathbf{f}_0$ the current measure. This model has been validated experimentally (see Sect. VI).

The core part of the *following* WPG is impedance (13). Impedance control has been discussed in the literature several times since [43]. Recently, [44] discusses it in the context of collaborative carrying between mobile manipulators. The interested reader can refer to these for a more in depth discussion on impedance control. Here, it suffices to say that (13) imposes a relation between (interaction) force and (CoM) motion, which is a mechanical impedance. The novelty here is in using impedance control in an MPC framework together with balance constraints for walking (14). Although its fidelity (i.e., maintaining the imposed force-motion relation) has been shown in [30], it has inherent limits due to the balance constraint (which takes priority). The main limiting factor in the QP (14) is the allowable instantaneous force change given the ZMP constraints. With some assumptions, this can be derived from the ZMP equation (3) as shown in [45]. Then, if the change in applied force is below such allowable limit, the robot can adjust its posture to handle the sustained force as shown in the simulations of [30] where up to $150N$ are applied to the robot.

2) Walking pattern generator for a leader robot:
For leading, a clear intention is necessary. The robot should track a reference trajectory, known beforehand. For collaborative carrying, this can be generated by knowing where the object is and where it will be transported to. A classic way for tracking a trajectory in operational space [46] is:

$$\ddot{\mathbf{c}}^{x,y} = \ddot{\mathbf{c}}_{\text{ref}}^{x,y} + \mathbf{B}(\dot{\mathbf{c}}_{\text{ref}}^{x,y} - \dot{\mathbf{c}}^{x,y}) + \mathbf{K}(\mathbf{c}_{\text{ref}}^{x,y} - \mathbf{c}^{x,y}), \tag{15}$$

where $\mathbf{B}$ and $\mathbf{K}$ are diagonal gain matrices with positive elements. This can be reformulated as an objective function, with an appropriate gain matrix, similar to that of the follower:

$$\left\|\mathbf{G}_{\text{bk}}(\tilde{\mathbf{c}}_{\text{ref}} - \tilde{\mathbf{c}})\right\|^2 = \left\|\mathbf{G}_{\text{bk}}\tilde{\mathbf{c}}_{\text{ref}} - \mathbf{G}_{\text{bk}}\mathbf{S}\mathbf{x} - \mathbf{G}_{\text{bk}}\mathbf{s}\right\|^2. \tag{16}$$

Furthermore, with the robot acting as leader, the external wrench should be included in the optimization argument, expanding it as $\mathbf{x} = [\tilde{\mathbf{u}}^\top\ \tilde{\mathbf{r}}^\top\ \tilde{\mathbf{f}}^\top]^\top$. The idea is that placing a part of the external wrench in the argument allows the robot to use the interaction to balance itself. However, for safety, $\tilde{\mathbf{f}}$ should be bounded and minimized.

The optimization problem, including again objectives (6), (7), and constraints (8), (10), becomes:

$$\begin{aligned}\underset{\mathbf{x}}{\text{argmin}} \quad & w_{\text{com}}\left\|\tilde{\mathbf{u}}\right\|^2 + w_{\text{zmp}}\left\|\tilde{\mathbf{z}}\right\|^2 + w_{\text{f}}\left\|\tilde{\mathbf{f}}\right\|^2 \\ & + w_{\text{lea}}\left\|\mathbf{G}_{\text{bk}}\tilde{\mathbf{c}}_{\text{ref}} - \mathbf{G}_{\text{bk}}\mathbf{S}\mathbf{x} - \mathbf{G}_{\text{bk}}\mathbf{s}\right\|^2 \\ \text{subject to} \quad & \underline{\tilde{\mathbf{z}}} \leq \tilde{\mathbf{z}} \leq \overline{\tilde{\mathbf{z}}} \\ & \underline{\tilde{\mathbf{r}}} \leq \tilde{\mathbf{r}} \leq \overline{\tilde{\mathbf{r}}} \\ & \underline{\tilde{\mathbf{f}}} \leq \tilde{\mathbf{f}} \leq \overline{\tilde{\mathbf{f}}}.\end{aligned} \tag{17}$$

Since $\tilde{\mathbf{f}}$ is now part of the argument, objectives and constraints are still of the forms (1) and (2b), respectively.

C. Feasibility and stability of the MPC

To conclude this section, we provide some insight into the feasibility of the QP problems (14) and (17). It has already been reported in [47] that the nominal MPC for walking with

[1]Throughout this paper, we denote with $\underline{x}$ and $\overline{x}$ lower and upper bounds (respectively) of variable x.

fixed footstep positions and without external forces is always feasible. It can be easily demonstrated that this property retains for the MPC formulations presented here. Perpetual feasibility, however, does not guarantee that the generated CoM motion does not diverge, leading to robot fall.

The standard approach to avoid divergence in MPC is to approximate an infinite preview horizon [48], for instance:

- It is possible to impose a terminal, so-called *capturability*, constraint to ensure that within a particular preview horizon the system can be stopped [49], [50]. Such constraint effectively prevents divergence, but may lead to infeasibility of the considered optimization problems. A detailed discussion of this topic can be found in [51].
- The second option is to use a "long enough" preview horizon, as justified in [52]. A bulk of previous works [11], [19], [22], [42], [53], [54], [55] validated this approach in practice and reached a consensus on the length of the preview horizon, which should span 2 footsteps.

We have chosen to use the second approach for the sake of simplicity and it was proven to be sufficient. In future works, however, it may be interesting to study the possibility of using a terminal constraint to allow the robot to resist excessive force applied by the human. For example, while following the human using (14), the robot may be led to a fall. In this case, switching to (17) would allow the robot to regain balance by resisting the human.

V. Whole-body control for collaborative carrying

The previous sections provided important building blocks for the collaborative carrying task. This section aims at wrapping everything together into coordinated whole-body motions. For instance, to generate the described walks, the WPG results: $\tilde{\mathbf{c}}$, $\tilde{\mathbf{r}}$, and $\mathbf{r}_{\text{sw}}$ (respectively: CoM trajectory, footprints, and swing foot trajectory) must be mapped to robot joint commands, $\mathbf{q}$. To explain how this is done, we start by recalling the optimization-based whole-body control framework developed in our research group [32]. Next, recurrent objectives and constraints are presented. Finally, we explain how all the components are assembled to realize the collaborative carrying.

A. Whole-body control as an optimization problem

To start detailing our whole-body control framework, we define the optimization argument in (2) as:

$$\mathbf{x} = \begin{bmatrix} \ddot{\mathbf{q}} \\ \boldsymbol{\lambda} \end{bmatrix}. \tag{18}$$

Here, $\mathbf{q}$ defines the robot configuration, i.e. the joint positions along with the floating-base representation [56], and $\boldsymbol{\lambda}$ is the vector of linearized friction cone base weights. This is defined so that all contact forces stacked in a column vector yield:

$$\mathbf{f}_{\text{con}} = \mathbf{K}_{\text{fc}}\boldsymbol{\lambda}, \tag{19}$$

with $\mathbf{K}_{\text{fc}} \in \mathbb{R}^{3n \times nm}$ a matrix of generators for linearizing the friction cone (n is the number of contact points, m the number of generators for linearization).

For each state (i.e., subtask) of the FSM of Fig. 2, we solve the following optimization problem:

$$\begin{aligned} \underset{\mathbf{x}}{\text{argmin}} \quad & \sum_j w_{\text{j}} f_{\text{base,j}}(\mathbf{x}) + \sum_k w_{\text{k}} f_{\text{spec,k}}(\mathbf{x}) \\ \text{subject to} \quad & \mathbf{A}_{\text{base}}\mathbf{x} \leq \mathbf{b}_{\text{base}} \\ & \mathbf{A}_{\text{spec}}\mathbf{x} \leq \mathbf{b}_{\text{spec}}. \end{aligned} \tag{20}$$

In Section V-B, we present the objectives and constraints that are recurrent in the collaborative carrying FSM, specifically the *tracking* and *set-point objectives*, and the *contact constraint*. Then, the *base* objective functions and constraints, which are applied at all states of the FSM, are detailed in Sect. V-C. Instead, the collection of objectives f_{spec} *specific* to each FSM state, will be described, along with the specific constraints, in Section V-D.

B. Reusable objectives and constraints

Several objectives and constraints are recurrent in the FSM, and can be written in re-usable form. For this, let us first define a task vector in the operational space $\mathbf{e}$ (e.g., the pose of any frame on the robot or on the carried object), and the function mapping it to robot joint space:

$$\mathbf{e} = f_{\mathbf{e}}(\mathbf{q}). \tag{21}$$

Assuming $f_{\mathbf{e}}$ is twice differentiable, and naming $\mathbf{J}_{\mathbf{e}}$ the task Jacobian:

$$\dot{\mathbf{e}} = \mathbf{J}_{\mathbf{e}}\dot{\mathbf{q}}, \tag{22}$$

$$\ddot{\mathbf{e}} = \mathbf{J}_{\mathbf{e}}\ddot{\mathbf{q}} + \dot{\mathbf{J}}_{\mathbf{e}}\dot{\mathbf{q}}, \tag{23}$$

we define the *tracking task objective* as:

$$\begin{aligned} & f_{\text{tr}}(\mathbf{x}, \mathbf{e}_{\text{des}}(t)) = \\ & \frac{1}{2}\left\|\mathbf{K}(\mathbf{e}_{\text{des}} - \mathbf{e}) + \mathbf{B}(\dot{\mathbf{e}}_{\text{des}} - \dot{\mathbf{e}}) + (\ddot{\mathbf{e}}_{\text{des}} - \ddot{\mathbf{e}})\right\|^2, \end{aligned} \tag{24}$$

where $\mathbf{e}_{\text{des}}(t)$ denotes the desired task trajectory (i.e., it includes $\mathbf{e}_{\text{des}}, \dot{\mathbf{e}}_{\text{des}}$ and $\ddot{\mathbf{e}}_{\text{des}}$), and $\mathbf{K}$ and $\mathbf{B}$ are square diagonal gain matrices with positive values. These can be tuned by considering the task dynamics equivalent to those of a mass-spring-damper system with unit mass. Typically, to obtain a critically damped system, only $\mathbf{K}$ needs to be tuned, with $\mathbf{B} = 2\sqrt{\mathbf{K}}$. Using (22) and (23), (24) can be written as (2a).

A particular case of the tracking task is the *set-point objective*, where only the reference position is considered, while the reference velocity and acceleration are set to zero:

$$f_{\text{sp}}(\mathbf{x}, \mathbf{e}_{\text{des}}) = \frac{1}{2}\left\|\mathbf{K}(\mathbf{e}_{\text{des}} - \mathbf{e}) - \mathbf{B}\dot{\mathbf{e}} - \ddot{\mathbf{e}}\right\|^2. \tag{25}$$

Apart from servoing a body part, another common goal is to keep a certain body part motionless. A common example is to keep the feet in contact with the ground. To this end, we define a *contact constraint*, by nullifying the acceleration of a robot point that is in contact with the environment:

$$\ddot{\mathbf{e}} = \mathbf{0}. \tag{26}$$

Using (23), this can be written as the equality constraint:

$$\begin{bmatrix} \mathbf{J}_{\mathbf{e}} & \mathbf{0} \end{bmatrix} \mathbf{x} = -\dot{\mathbf{J}}_{\mathbf{e}}\dot{\mathbf{q}}. \tag{27}$$

C. Base objectives and constraints

1) Base objective functions:

The first base objective function is termed the *posture task*, and represented as f_{pos}. This corresponds to positioning joints at a given posture $\mathbf{q}_{\text{des}}$, with null $\dot{\mathbf{q}}_{\text{des}}$ and $\ddot{\mathbf{q}}_{\text{des}}$:

$$f_{\text{pos}}(\mathbf{x}, \mathbf{q}_{\text{des}}) = \frac{1}{2} \left\| \mathbf{K}(\mathbf{q}_{\text{des}} - \mathbf{q}) - \mathbf{B}\dot{\mathbf{q}} - \ddot{\mathbf{q}} \right\|^2, \tag{28}$$

with $\mathbf{K}$ and $\mathbf{B}$ square diagonal gain matrices with positive values. Note that this is a typical example of set-point task (25), obtained with $\mathbf{e} = \mathbf{q}$. Exposing the joint accelerations via numerical integration at each time interval k of duration Δt:

$$\begin{aligned} \dot{\mathbf{q}}_{k+1} &= \dot{\mathbf{q}}_k + \ddot{\mathbf{q}}_k \Delta t, \\ \mathbf{q}_{k+1} &= \mathbf{q}_k + \dot{\mathbf{q}}_k \Delta t + \frac{1}{2} \ddot{\mathbf{q}}_k \Delta t^2, \end{aligned} \tag{29}$$

it is straightforward to show that objective (28) is of the form (2a). The goal of the posture task is to have a *default* configuration of each joint. Hence, its weight w_{pos} normally has a low value, to give priority to more important tasks. The second base objective consists in minimizing $\|\boldsymbol{\lambda}\|^2$:

$$f_{\boldsymbol{\lambda}}(\mathbf{x}) = \|\boldsymbol{\lambda}\|^2 = \left\| \begin{bmatrix} \mathbf{0} & \mathbf{I} \end{bmatrix} \mathbf{x} \right\|^2. \tag{30}$$

As shown in [32], this objective function, joined with (28), allows an easier numeric solution to the QP problem.

2) Base constraints:

There are four constraints in the base formulation of our optimization problem (20), namely:

$$\boldsymbol{\lambda} \geq \mathbf{0} \tag{31a}$$

$$\underline{\boldsymbol{\tau}} \leq \boldsymbol{\tau} \leq \overline{\boldsymbol{\tau}} \tag{31b}$$

$$\underline{\mathbf{q}} \leq \mathbf{q} \leq \overline{\mathbf{q}} \tag{31c}$$

$$\underline{\dot{\mathbf{q}}} \leq \dot{\mathbf{q}} \leq \overline{\dot{\mathbf{q}}}, \tag{31d}$$

$\boldsymbol{\tau}$ being the applied joint torques.

Firstly, (31a) ensures that the contact forces are inside the friction cone (no slipping). This can be formulated as:

$$\begin{bmatrix} \mathbf{0} & \mathbf{I} \end{bmatrix} \mathbf{x} \geq \mathbf{0}. \tag{32}$$

Second, (31b) places bounds on the torques $\boldsymbol{\tau}$. These can be obtained from the robot dynamic equation:

$$\boldsymbol{\tau} = \mathbf{H}\ddot{\mathbf{q}} + \mathbf{C}\dot{\mathbf{q}} + \boldsymbol{\tau}_{\mathbf{g}} - \mathbf{J}_{\text{con}}^{\top} \mathbf{f}_{\text{con}}, \tag{33}$$

with $\mathbf{H}$ and $\mathbf{C}$ respectively the inertia and Coriolis/centrifugal terms taking into account the floating-base [56], $\boldsymbol{\tau}_{\mathbf{g}}$ the torques due to gravity, $\mathbf{J}_{\text{con}}$ the stacked contact point Jacobian matrices, and $\mathbf{f}_{\text{con}}$ the stacked vector of contact forces from (19). The constraint can then be rewritten:

$$\underline{\boldsymbol{\tau}} - \mathbf{C}\dot{\mathbf{q}} - \boldsymbol{\tau}_{\mathbf{g}} \leq \begin{bmatrix} \mathbf{H} & -\mathbf{J}_{\text{con}}^{\top} \mathbf{K}_{\text{fc}} \end{bmatrix} \mathbf{x} \leq \overline{\boldsymbol{\tau}} - \mathbf{C}\dot{\mathbf{q}} - \boldsymbol{\tau}_{\mathbf{g}}. \tag{34}$$

The third and fourth constraints, (31c) and (31d), bound joint positions and velocities. With (29), these become:

$$\underline{\dot{\mathbf{q}}} - \dot{\mathbf{q}} \leq \begin{bmatrix} \mathbf{I}\Delta t & \mathbf{0} \end{bmatrix} \mathbf{x} \leq \overline{\dot{\mathbf{q}}} - \dot{\mathbf{q}}, \tag{35a}$$

$$\underline{\mathbf{q}} - \mathbf{q} - \dot{\mathbf{q}}\Delta t \leq \frac{1}{2} \begin{bmatrix} \mathbf{I}\Delta t^2 & \mathbf{0} \end{bmatrix} \mathbf{x} \leq \overline{\mathbf{q}} - \mathbf{q} - \dot{\mathbf{q}}\Delta t. \tag{35b}$$

Stacking (32), (34), (35a) and (35b), yields the explicit expressions of $\mathbf{A}_{\text{base}}$, and $\mathbf{b}_{\text{base}}$ in (20).

D. Specific objectives and constraints of each FSM state

Here we detail the objectives and constraints specific to each FSM state. An important aspect concerns the control of the CoM. In walking FSM states (DS, RSS and LSS), this is servoed using a *tracking task objective* (24) to follow the CoM trajectory output by the WPG (leader or follower).

That is, $\mathbf{c}_{\text{des}}(t)$ and $\mathbf{r}_{\text{swdes}}(t)$ are both generated by the WPG detailed in Sect. IV. For all other FSM states, we use a *set-point objective* (25) to attract the CoM towards the middle of the two feet by setting $\mathbf{c}_{\text{des}}$ accordingly.

1) Double support:

During the Double Support (DS) states, both feet: $\mathbf{r}_{\text{left}}, \mathbf{r}_{\text{right}}$, must maintain contact with the ground, via *contact constraints*. The CoM is servoed with a trajectory $\mathbf{c}_{\text{des}}(t)$, obtained from the standard WPG of Section IV.

In summary, the whole-body optimization problem is:

$$\begin{aligned} \underset{\mathbf{x}}{\text{argmin}} \quad & w_{\text{c}} f_{\text{tr}}(\mathbf{x}, \mathbf{c}_{\text{des}}(t)) + w_{\text{pos}} f_{\text{pos}}(\mathbf{x}, \mathbf{q}_{\text{des}}) + w_{\boldsymbol{\lambda}} f_{\boldsymbol{\lambda}}(\mathbf{x}), \\ \text{subject to} \quad & \ddot{\mathbf{r}}_{\text{left}} = \mathbf{0}, \\ & \ddot{\mathbf{r}}_{\text{right}} = \mathbf{0}, \\ & \mathbf{A}_{\text{base}} \mathbf{x} \leq \mathbf{b}_{\text{base}}. \end{aligned} \tag{36}$$

2) Right/left single support:

While walking, single support states (RSS or LSS) occur between two consecutive double support states. As such, they retain the CoM trajectory tracking task from the standard WPG. Differently from DS, only one foot supports the weight and is constrained to the ground, while the other (swinging) is servoed in the air to track $\mathbf{r}_{\text{swdes}}(t)$ (any swing foot desired trajectory). Hence, the optimization problem is:

$$\begin{aligned} \underset{\mathbf{x}}{\text{argmin}} \quad & w_{\text{c}} f_{\text{tr}}(\mathbf{x}, \mathbf{c}_{\text{des}}(t)) + w_{\text{sw}} f_{\text{tr}}(\mathbf{x}, \mathbf{r}_{\text{swdes}}(t)) + \\ & w_{\text{pos}} f_{\text{pos}}(\mathbf{x}, \mathbf{q}_{\text{des}}) + w_{\boldsymbol{\lambda}} f_{\boldsymbol{\lambda}}(\mathbf{x}), \\ \text{subject to} \quad & \ddot{\mathbf{r}}_{\text{sup}} = \mathbf{0}, \\ & \mathbf{A}_{\text{base}} \mathbf{x} \leq \mathbf{b}_{\text{base}}. \end{aligned} \tag{37}$$

3) Pregrasping, squeezing and releasing:

The *pregrasp*, *squeeze* and *release* states have the same formulation, the only difference being their preceding state. Thus, without loss of generality, we only present the pregrasp. The *pregrasp* state is a waypoint state that eases the grasping by targeting a set of n preplanned pregrasp point locations, $\{\mathbf{p}_{\text{grdes, 1}} \dots \mathbf{p}_{\text{grdes, n}}\}$. The synthesis of these locations can be formalized either as a stance generation problem [57], or by considering caging [58]. Here, we assume that a set of stable grasp point locations is given, along with the corresponding pregrasp stance, according to the chosen instance of the taxonomy (*grasp type*, see Section II). For instance, we design the body grasps shown in Fig. 3 for the *pipe-shoulder* and *pipe-front* examples of Fig. 1. In those cases, we parametrize the grasp via the contact frames shown in Fig. 3. More generally, we define n operational frames on the robot body. The pose of each one, denoted by: $\mathbf{p}_{\text{gr, i}}$ $(i = 1 \dots n)$, should be servoed to a desired pose: $\mathbf{p}_{\text{grdes, i}}$. This corresponds to n set-point objectives (25). Note, from Fig. 2, that pre-grasp and release are only performed when the robot is standing, in double support. Thus, both foot contact constraints are

added as well as the set point task on the CoM that is needed to maintain balance. In summary, the pregrasp, squeeze, and release optimization problems can all be formulated as:

$$\begin{aligned} \underset{\mathbf{x}}{\text{argmin}} \quad & \sum_{i=1}^{n} w_{\text{gr,i}} f_{\text{sp,i}}(\mathbf{x}, \mathbf{p}_{\text{grdes, i}}) + w_{\text{c}} f_{\text{sp}}(\mathbf{x}, \mathbf{c}_{\text{des}}) + \\ & w_{\text{pos}} f_{\text{pos}}(\mathbf{x}, \mathbf{q}_{\text{des}}) + w_{\boldsymbol{\lambda}} f_{\boldsymbol{\lambda}}(\mathbf{x}), \\ \text{subject to} \quad & \ddot{\mathbf{r}}_{\text{left}} = \mathbf{0}, \\ & \ddot{\mathbf{r}}_{\text{right}} = \mathbf{0}, \\ & \mathbf{A}_{\text{base}}\mathbf{x} \leq \mathbf{b}_{\text{base}}. \end{aligned} \tag{38}$$

4) Holding the object while lifting, carrying, placing it: After having successfully squeezed the object, a grasp is maintained by the *hold* state. We chose to formalize this via null motion constraints between the grasping points on the robot body. In principle, it is possible to constrain all permutations of contact pairs. However, this results in numerical problems for the solver, if the closed kinematic chains are not handled properly. Instead, we only use $n-1$ constraints, defined by all pairs of points $(i, i+1)$, with $i = 1, \ldots, n-1$. This approach does not impede changes in object configurations (e.g., motions while holding), but ensures that the grasp form is maintained. This principle comes from caging [58] where the object being caged moves together with a properly formed cage. Once the object is held, it can be considered as part of the robot. We can then define an operational frame related to the object, $\mathbf{o}$, and servo its pose via a set-point task $f_{\text{sp}}(\mathbf{x}, \mathbf{o}_{\text{des}})$. We assume here that $\mathbf{o}_{\text{des}}$ is provided beforehand, for example by a high-level plan (as for the grasp points in Section V-D3). For collaborative carrying, the hold state is to be realized while *lifting*, *walking* (RSS, DS, LSS), and *placing* (see Fig. 2).

For *holding while lifting* and *holding while placing*, the optimization problem is:

$$\begin{aligned} \underset{\mathbf{x}}{\text{argmin}} \quad & w_{\text{o}} f_{\text{sp}}(\mathbf{x}, \mathbf{o}_{\text{des}}) + w_{\text{c}} f_{\text{sp}}(\mathbf{x}, \mathbf{c}_{\text{des}}) + \\ & w_{\text{pos}} f_{\text{pos}}(\mathbf{x}, \mathbf{q}_{\text{des}}) + w_{\boldsymbol{\lambda}} f_{\boldsymbol{\lambda}}(\mathbf{x}), \\ \text{subject to} \quad & \ddot{\mathbf{p}}_{\text{gr,1}} - \ddot{\mathbf{p}}_{\text{gr,2}} = \mathbf{0}, \\ & \vdots \\ & \ddot{\mathbf{p}}_{\text{gr,n-1}} - \ddot{\mathbf{p}}_{\text{gr,n}} = \mathbf{0}, \\ & \ddot{\mathbf{r}}_{\text{left}} = \mathbf{0}, \\ & \ddot{\mathbf{r}}_{\text{right}} = \mathbf{0}, \\ & \mathbf{A}_{\text{base}}\mathbf{x} \leq \mathbf{b}_{\text{base}}. \end{aligned} \tag{39}$$

For *holding during double support*, the optimization problem is similar, except that $w_{\text{c}} f_{\text{sp}}(\mathbf{x}, \mathbf{c}_{\text{des}})$ is replaced by $w_{\text{c}} f_{\text{tr}}(\mathbf{x}, \mathbf{c}_{\text{des}}(t))$, with $\mathbf{c}_{\text{des}}(t)$ output by either the follower or leader WPG. Therefore, the optimization problem is:

$$\begin{aligned} \underset{\mathbf{x}}{\text{argmin}} \quad & w_{\text{o}} f_{\text{sp}}(\mathbf{x}, \mathbf{o}_{\text{des}}) + w_{\text{c}} f_{\text{tr}}(\mathbf{x}, \mathbf{c}_{\text{des}}(t)) + \\ & w_{\text{pos}} f_{\text{pos}}(\mathbf{x}, \mathbf{q}_{\text{des}}) + w_{\boldsymbol{\lambda}} f_{\boldsymbol{\lambda}}(\mathbf{x}), \\ \text{subject to} \quad & \ddot{\mathbf{p}}_{\text{gr,1}} - \ddot{\mathbf{p}}_{\text{gr,2}} = \mathbf{0}, \\ & \vdots \\ & \ddot{\mathbf{p}}_{\text{gr,n-1}} - \ddot{\mathbf{p}}_{\text{gr,n}} = \mathbf{0}, \\ & \ddot{\mathbf{r}}_{\text{left}} = \mathbf{0}, \\ & \ddot{\mathbf{r}}_{\text{right}} = \mathbf{0}, \\ & \mathbf{A}_{\text{base}}\mathbf{x} \leq \mathbf{b}_{\text{base}}. \end{aligned} \tag{40}$$

Finally, for *holding during single support*, the optimization problem is:

$$\begin{aligned} \underset{\mathbf{x}}{\text{argmin}} \quad & w_{\text{o}} f_{\text{sp}}(\mathbf{x}, \mathbf{o}_{\text{des}}) + w_{\text{c}} f_{\text{tr}}(\mathbf{x}, \mathbf{c}_{\text{des}}(t)) + \\ & w_{\text{sw}} f_{\text{tr}}(\mathbf{x}, \mathbf{r}_{\text{swdes}}(t)) + w_{\text{pos}} f_{\text{pos}}(\mathbf{x}, \mathbf{q}_{\text{des}}) + \\ & w_{\boldsymbol{\lambda}} f_{\boldsymbol{\lambda}}(\mathbf{x}), \\ \text{subject to} \quad & \ddot{\mathbf{p}}_{\text{gr,1}} - \ddot{\mathbf{p}}_{\text{gr,2}} = \mathbf{0}, \\ & \vdots \\ & \ddot{\mathbf{p}}_{\text{gr,n-1}} - \ddot{\mathbf{p}}_{\text{gr,n}} = \mathbf{0}, \\ & \ddot{\mathbf{r}}_{\text{sup}} = \mathbf{0}, \\ & \mathbf{A}_{\text{base}}\mathbf{x} \leq \mathbf{b}_{\text{base}}. \end{aligned} \tag{41}$$

Again, $\mathbf{c}_{\text{des}}(t)$ can be output by the follower or leader WPG.

E. Note on feasibility

As indicated in Section III, conflicts may arise between the QP constraints. Although constraint relaxation is a viable strategy to recover from infeasibility, it may result in control inputs which are either physically inconsistent, or not executable by the hardware. Other strategies are detailed below.

Object handling motions –pregrasping, squeezing, and releasing– are defined with the help of a contact stance planner as in [32], [57]. Since this planner guarantees feasibility only at specific postures, we have to verify, through simulations, that the interpolated motions are also feasible. For example, the second scenario from below in Fig. 1 turned out to be unfeasible on our humanoid, because of the body grasp configuration.

Walking may not be feasible due to discrepancies between the reduced model employed in the WPG and the whole body model, namely because of these WPG assumptions:

(a) absence of kinematic and joint limits;
(b) zero rate of angular momentum;
(c) constant vertical component of the external force.

Issues of such kind are traditionally addressed with *proxy* constraints, which reflect limitations of the reduced model [59]. All the constraints in the WPG can be seen as proxies:

- bounds on the ZMP positions are chosen depending on the size of the feet, while *safety margins* in these constraints implicitly account for (b);
- feasible regions for the landing foot positions address kinematic limits in (a) and can be estimated using simulations as in [60];

- bounds on the external wrench reflect dynamic limits in (a) and can also be chosen empirically in simulations.

Although it is also possible to avoid assumption (c) as in [61], or to address (b) using a reduced model from [40], the three proxy constraints presented above were sufficient in this work.

VI. Experiments and Results

This section shows how we validated the proposed framework, first in dynamic simulations, and then with experiments on an HRP-4 humanoid from Kawada Industries, with customized ATI Mini40 force/torque sensors in the wrists. The robot is position controlled, with joint setpoints updated every 5ms by the whole body controller described in Section V. In all experiments, for the walk, we set the swing duration to $t_{\text{swf}} = 0.7$s, and the stepping height to $r_{\text{sth}} = 0.07$m. The average forward walking velocity, in the leader CoM trajectory (15), is set to 0.1m.s^{-1}. All simulations are run with the same general parameters and timing constraints as on the real robot, using a 2.7 GHz i7 processor.

A. Simulations

The base functionality of the WPG accounting for external wrench was previously verified and tested, with the results presented in [30]. Complementary to those results, we concentrate on the implications of carrying an object together with a human. Specifically, due to the carried object weight, a negative force component in the z direction will be present. Equation (3) shows that an important negative f^z_{ext} will increase the robustness to external wrenches in x and y directions, by reducing their net effect on the ZMP. Furthermore, if f^z_{ext} is comparable to the robot weight, it reduces the acceleration effects. An intuitive way to interpret this is that the added weight lowers the CoM of the combined (robot and object) system, as shown in Fig. 5. Here, a 150N force is pulling the robot forward. To compensate it, the WPG produces a posture change. On the right image, a 500N weight is also added. The end result is a less drastic posture change output by the WPG. From this, we see that carrying heavier objects actually helps the humanoid stability (assuming the robot motors can handle the extra load).

Concerning whole body control, we present simulations on the designed *pregrasp* and *squeezing* postures output by (38). For these, we must define the control frame poses $\mathbf{p}_{\text{gr, i}}$ on the surface of the robot body parts (e.g. shoulder, chest, hands, etc.), and compute the corresponding Jacobians. Some postures have been shown in Fig. 3. However, due to hardware issues (broken wrist joint), we also had to design *one-handed* versions of these, shown in Fig. 6, along with a grasping motion of the hand (bottom figures). On the HRP-4 hand, the thumb is controlled by one motor, and the four other fingers are actuated together by a second motor. Hence, the four fingers open and close together during squeezing, and this motion is defined by a single *joint position*. Another point of interest is the left arm motion in the front-wrap squeezing (middle right in Fig. 6). This is caused by objective function $f_{\text{sp}}(\mathbf{x}, \mathbf{c}_{\text{des}})$ in (38)), which keeps the ground projection of the CoM near the center of the support polygon. Since the squeeze motion moves the chest frame forward, the QP solver uses the left arm to realize this objective.

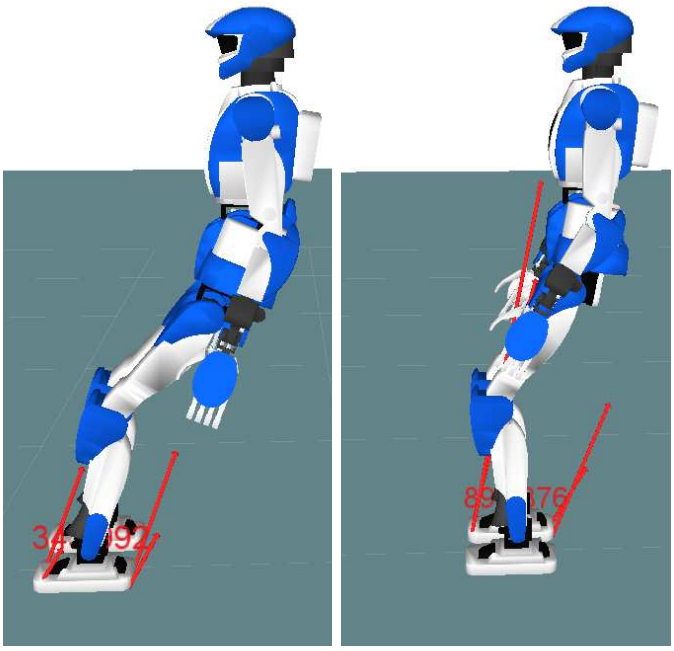

Fig. 5. Screenshots of two simulations with 150N force pulling the robot forward. In the simulation on the right, a downward vertical force component of 500N is also added.

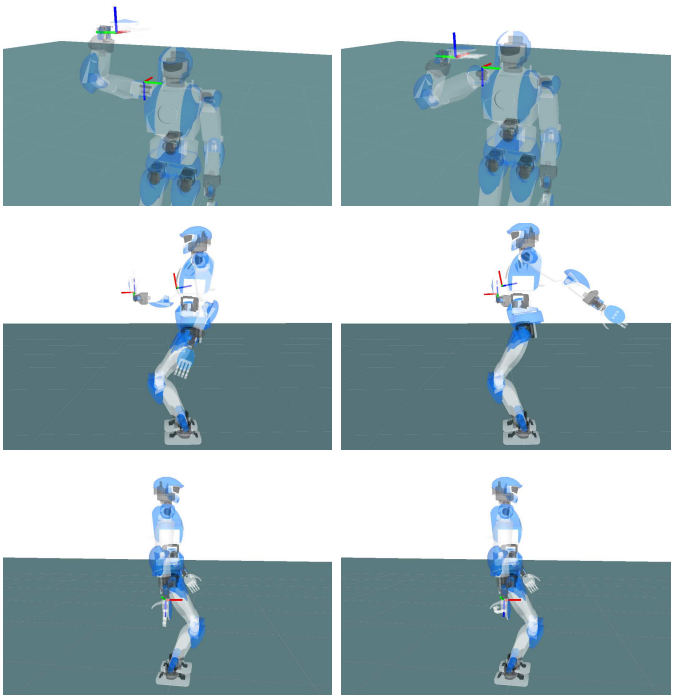

Fig. 6. One-handed pregrasp (left) and squeezing (right). Top to bottom: shoulder-mounted body grasp, front-wrap body grasp, and right hand grasp.

For integrating the walk and the whole-body controller, recall that at each instant the WPG (be it follower (14) or leader (17)) provides a reference CoM position, velocity and acceleration. In Fig. 7, we compare the CoM and ZMP

positions, as requested by the WPG (here: *leader*, with no external forces) and as achieved by the whole body controller. The plot shows that the CoM is tracked well enough and that the robot is actually walking at 0.1m.s^{-1}, as requested. As for the ZMP, the approximation of null angular momentum rate leads to the slight tracking error visible in the figure. Nevertheless, our tests (both dynamic simulations and real experiments) show that this ZMP tracking error does not affect robot balance.

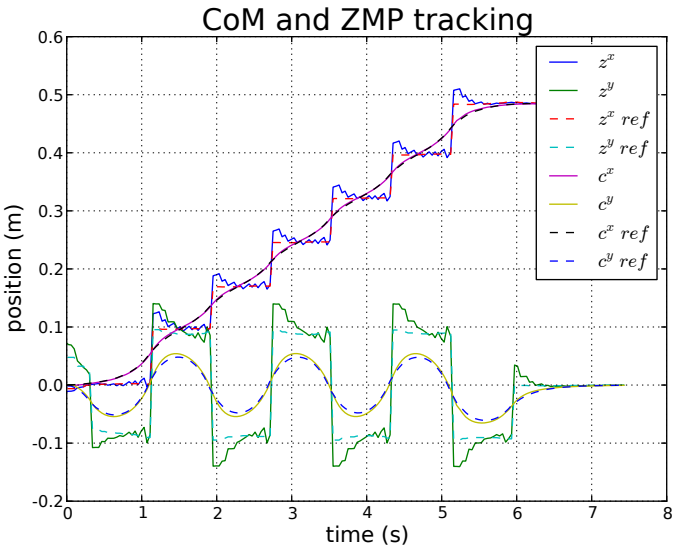

Fig. 7. Tracking task of the CoM using the WPG-generated reference CoM along with a comparison of the resulting ZMP.

Lastly, we present simulations of walking as *leader*, while holding (Section V-D4). Image sequences of walking while holding using two-handed front-wrap, and shoulder-mounted body grasps, are respectively shown in Figures 8 and 9. Although only some chosen examples are illustrated, either of the two WPG may be used, along with any of the grasps. These examples demonstrate that we are capable of properly servoing the CoM, while maintaining the desired robot posture.

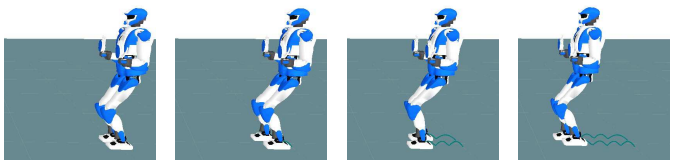

Fig. 8. Walking while holding, using a front-wrap body grasp.

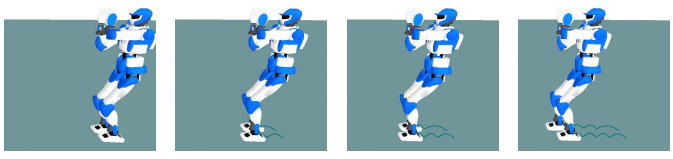

Fig. 9. Walking while holding, using a shoulder-mounted body grasp.

B. Real robot experiments

After having verified the framework in simulation, we moved on to experiments on the real HRP-4. Representative tests are shown in the video, attached to this paper, and available at: https://youtu.be/lHG4AbAvt_4. Screenshots are also shown in Fig. 10. The figure shows (left to right, top then bottom): shoulder-mounted box carrying as leader, front-wrap box carrying as leader, hand grasped stretcher carrying as follower, and hand grasped bucket carrying as follower. These correspond to four of the six examples introduced in Fig. 1. All four collaborative carrying scenarios were successful, with the robot acting as both leader and follower. For the two missing examples: first, table carrying (first scenario in Fig. 1) was validated in our previous work [19], [22], [27], [55]; second, the example requiring a side body grasp (fifth scenario in Fig. 1) is kinematically infeasible for HRP-4, as stated in Section V-E.

Fig. 10. Experiments with HRP-4 carrying various objects with a human. Top: $15N$ carton box, bottom left: $13N$ stretcher, bottom right: $8N$ bucket

Relevant data from the stretcher carrying task, with the robot walking as follower (bottom left in Fig. 10), are shown in Fig. 11. The top plot shows the CoM and ZMP reference signals, generated by the WPG (14), together with the measured values. A significant difference, due to impact, is only observed on contact transitions (footsteps). Meanwhile, the bottom figure shows the forward (pulling) component of the interaction force, measured by the two wrist force sensors, and then low-pass filtered and transformed to the CoM frame, $f^{\text{x}}_{\text{ext}}$. Note the pause in the walk (top figure), around the 13 to 15 second mark, corresponding to a strong decrease of interaction force (since the human stopped). Throughout the experiment, the CoM and ZMP reference values are properly adapted to the external force, as the robot follows the human.

Furthermore, Fig. 12 shows the raw force/torque sensor data in the corresponding force sensor frames. In such frames, the x component roughly corresponds to the object weight, showing the robot is carrying around $10N$ per hand throughout the experiment. According to our prior calibration data, each hand weighs $7N$. Therefore, the robot is supporting a total of $6N$ of the stretcher weight which is about $13N$, hence it is approximately sharing the load with the human. The y

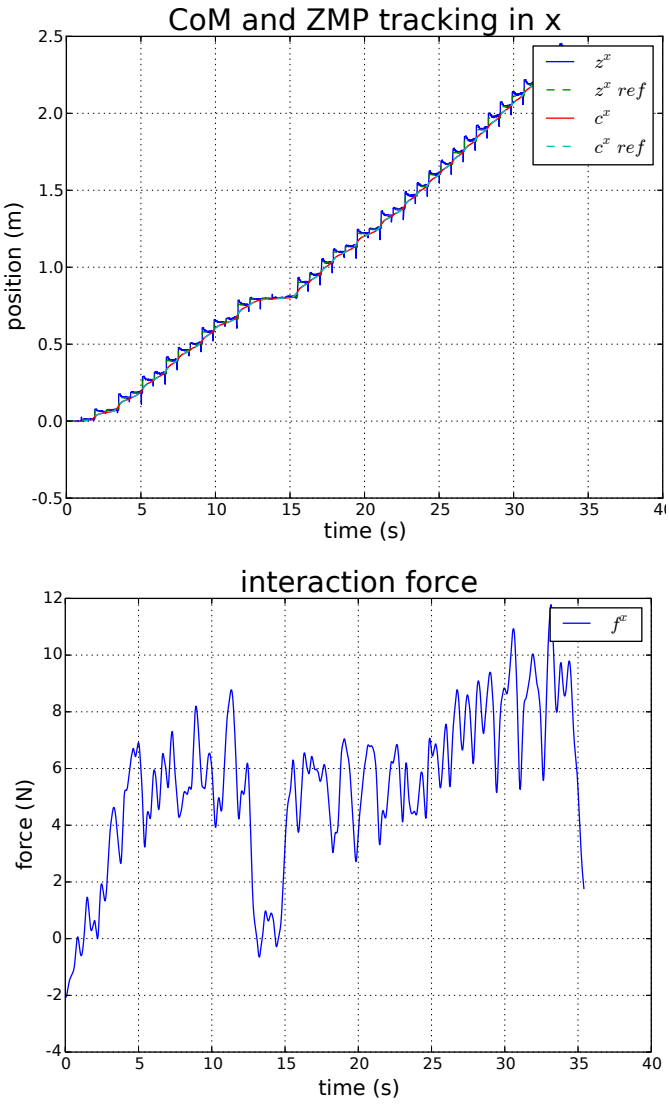

Fig. 11. Data from a stretcher carrying scenario with the robot walking as a follower. Top: reference and actual CoM and ZMP (as generated by the WPG). Bottom: forward (pulling) component of the interaction force.

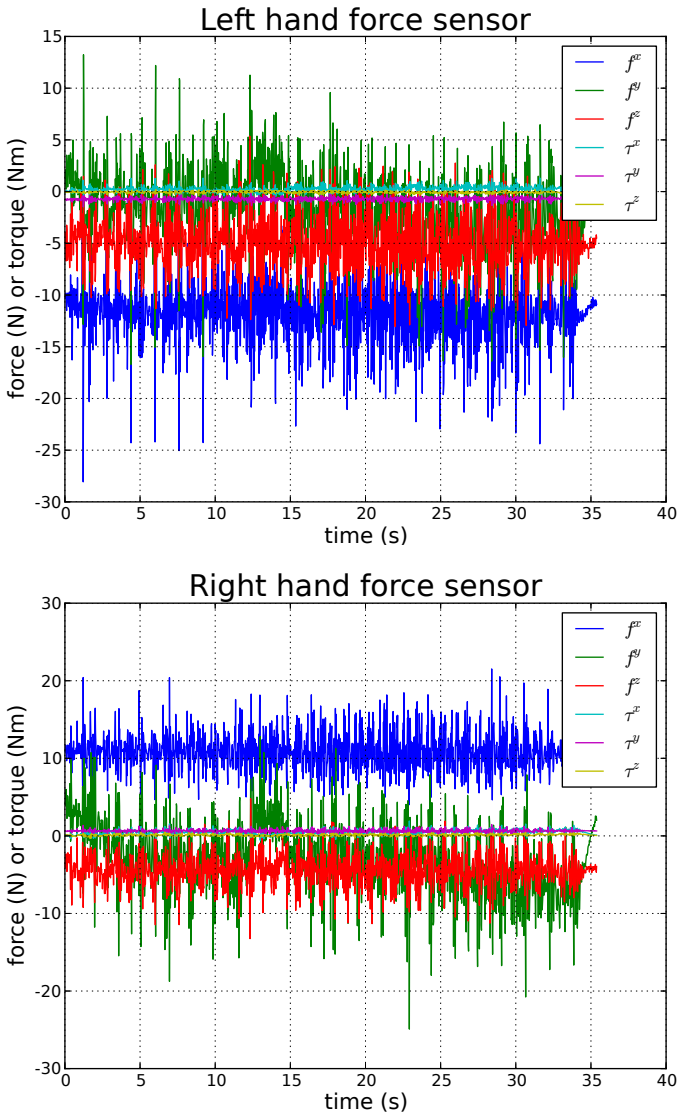

Fig. 12. Raw force/torque sensor data from a stretcher carrying scenario with the robot walking as a follower. Top: left hand. Bottom: right hand.

component roughly corresponds to the previously discussed interaction force in Fig. 11. Finally, the z component coincides with the grasping forces applied on the stretcher in between both hands. This remains around $5N$ throughout the test.

These results show that the overall approach works well, although force sensing is available only at the robot wrists, and not at the other contact points (e.g., on the shoulder and chest). The grasp stability could be improved, if force/contact sensing was available on other body parts.

VII. Conclusion

This article explores several aspects of human-humanoid collaborative carrying. We started by looking at this task as a whole, to infer the core principles, in order to program them on a humanoid robot. To this end, we created a Finite State Machine, encompassing all of the necessary subtasks. Next, we revisited locomotion and balance in relation to physical interaction. For this, we designed two walking pattern generators that not only take into account the physical interaction constraints, but also use them accordingly, to operate as a follower or leader. Then, we discussed how all of this can be designed as objectives and constraints of an optimization problem for a whole-body controller. We finally presented simulations and real test cases on the HRP-4 humanoid.

Although our approach proved successful, there are still several areas that can be largely improved with future works. Firstly, one key issue, outlined by the real experiments, is the need for force estimation. Related to this, we outlined the need for distributed force sensing on the entire robot body, instead of only on the wrist. Distributed tactile sensors can improve body grasps as tested with the HRP-2 in [62]. Another key improvement concerns the wrench prediction model for better proactive behaviors. A current limitation is that the wrench is simply predicted to be constant over the preview horizon. However, since we believe the framework is very well suited for including proactivity, a better perceptual model is necessary. This requires integrating human perception for intention recognition, a difficult challenge, but also an active

research area in physical human-robot interaction. Concerning the walk, although the WPG presented here is simplified, its core concepts do not conflict with improvements such as those in [63] which add robustness, allowing stair climbing. Another possible direction for future investigation in WPG design is addition of the terminal capturability constraint as indicated in Section IV-C. Apart from improving the WPG itself, its integration in whole-body control can also be improved, with works such as [49] which aims at combining the separate QPs. Lastly, a limiting factor for our real experiments was the low-level closed loop stabilizing controller of the HRP-4, which modifies the final joint references sent to the robot actuators [64]. To solve this, a dedicated stabilizer, consistent with our framework, should be designed. Finally, once the system is improved in terms of performance, user-related studies, with several different users (possibly also instrumented) is worthy of investigation.

REFERENCES

[1] K. Yokoyama, H. Handa, T. Isozumi, Y. Fukase, K. Kaneko, F. Kanehiro, Y. Kawai, F. Tomita, and H. Hirukawa, "Cooperative works by a human and a humanoid robot," in *IEEE Int. Conf. on Robotics and Automation*, vol. 3, pp. 2985–2991, 2003.

[2] K. Kosuge, M. Sato, and N. Kazamura, "Mobile robot helper," in *IEEE Int. Conf. on Robotics and Automation*, vol. 1, pp. 583–588, 2000.

[3] O. Khatib, "Mobile manipulation: The robotic assistant," *Robotics and Autonomous Systems*, vol. 26, no. 2–3, pp. 175–183, 1999.

[4] J. Stückler and S. Behnke, "Following human guidance to cooperatively carry a large object," in *IEEE-RAS Int. Conf. on Humanoid Robots*, pp. 218–223, 2011.

[5] M. Lawitzky, A. Mortl, and S. Hirche, "Load sharing in human-robot cooperative manipulation," in *IEEE Int. Symposium on Robot and Human Interactive Communication*, pp. 185–191, Sept 2010.

[6] H. Wang and K. Kosuge, "Control of a Robot Dancer for Enhancing Haptic Human-Robot Interaction in Waltz," *IEEE Transactions on Haptics*, vol. 5, no. 3, pp. 264–273, 2012.

[7] J. Lafaye, D. Gouaillier, and P. B. Wieber, "Linear model predictive control of the locomotion of Pepper, a humanoid robot with omnidirectional wheels," in *IEEE-RAS Int. Conf. on Humanoid Robots*, 2014.

[8] K. S. Kim, T. Llado, and L. Sentis, "Full-body collision detection and reaction with omnidirectional mobile platforms: a step towards safe human–robot interaction," *Autonomous Robots*, vol. 40 (2), pp. 325–341, 2016.

[9] E. Berger, D. Vogt, N. Haji-Ghassemi, B. Jung, and H. B. Amor, "Inferring guidance information in cooperative human-robot tasks," in *IEEE-RAS Int. Conf. on Humanoid Robots*, pp. 124–129, 2013.

[10] M. Bellaccini, L. Lanari, A. Paolillo, and M. Vendittelli, "Manual guidance of humanoid robots without force sensors: Preliminary experiments with NAO," in *IEEE Int. Conf. on Robotics and Automation*, 2014.

[11] T. Koolen, T. de Boer, J. Rebula, A. Goswami, and J. Pratt, "Capturability-based analysis and control of legged locomotion, Part 1: Theory and application to three simple gait models," *Int. Journal of Robotics Research*, vol. 31, no. 9, pp. 1094–1113, 2012.

[12] J. Pratt, T. Koolen, T. de Boer, J. Rebula, S. Cotton, J. Carff, M. Johnson, and P. Neuhaus, "Capturability-based analysis and control of legged locomotion, Part 2: Application to M2V2, a lower-body humanoid," *Int. Journal of Robotics Research*, vol. 31, no. 10, pp. 1117–1133, 2012.

[13] S. McGill and D. Lee, "Cooperative humanoid stretcher manipulation and locomotion," in *IEEE-RAS Int. Conf. on Humanoid Robots*, 2011.

[14] M.-H. Wu, S. Ogawa, and A. Konno, "Symmetry position/force hybrid control for cooperative object transportation using multiple humanoid robots," *Advanced Robotics*, vol. 30, no. 2, pp. 131–149, 2016.

[15] Y. Hirata and K. Kosuge, "Distributed robot helpers handling a single object in cooperation with a human," in *IEEE Int. Conf. on Robotics and Automation*, vol. 1, pp. 458–463 vol.1, 2000.

[16] W. Sheng, A. Thobbi, and Y. Gu, "An Integrated Framework for Human Robot Collaborative Manipulation," *IEEE Transactions on Cybernetics*, vol. 45, pp. 2030–2041, Oct 2015.

[17] R. Ikeura, H. Monden, and H. Inooka, "Cooperative motion control of a robot and a human," in *International Workshop on Robot and Human Communication*, (Nogoya, Japan), pp. 112–117, 18-20 July 1994.

[18] K. Reed and M. Peshkin, "Physical Collaboration of Human-Human and Human-Robot Teams," *IEEE Trans. on Haptics*, vol. 1 (2), pp. 108–120, 2008.

[19] A. Bussy, A. Kheddar, A. Crosnier, and F. Keith, "Human-humanoid haptic joint object transportation case study," in *IEEE/RSJ Int. Conf. on Intelligent Robots and Systems*, pp. 3633–3638, 2012.

[20] A. Mörtl, M. Lawitzky, A. Kucukyilmaz, M. Sezgin, C. Basdogan, and S. Hirche, "The role of roles: Physical cooperation between humans and robots," *Int. Journal of Robotics Research*, vol. 31, no. 13, pp. 1656–1674, 2012.

[21] P. Evrard and A. Kheddar, "Homotopy switching model for dyad haptic interaction in physical collaborative tasks," in *EuroHaptics Conference and Symposium on Haptic Interfaces for Virtual Environment and Teleoperator Systems*, pp. 45–50, IEEE, 2009.

[22] A. Bussy, P. Gergondet, A. Kheddar, F. Keith, and A. Crosnier, "Proactive behavior of a humanoid robot in a haptic transportation task with a human partner," in *IEEE Int. Symposium on Robot and Human Interactive Communication*, pp. 962–967, 2012.

[23] P. Evrard and A. Kheddar, "Homotopy switching model for dyad haptic interaction in physical collaborative tasks," in *IEEE International Symposium on Robot and Human Interactive Communication*, (Toyama, Japan), pp. 1–6, Sept. 27 2009-Oct. 2 2009.

[24] S. Ikemoto, H. B. Amor, T. Minato, B. Jung, and H. Ishiguro, "Physical Human-Robot Interaction: Mutual Learning and Adaptation," *IEEE Robotics Automation Magazine*, vol. 19, pp. 24–35, Dec 2012.

[25] J. R. Medina, T. Lorenz, and S. Hirche, "Synthesizing Anticipatory Haptic Assistance Considering Human Behavior Uncertainty," *IEEE Trans. on Robotics*, vol. 31, pp. 180–190, Feb 2015.

[26] C. E. Madan, A. Kucukyilmaz, T. M. Sezgin, and C. Basdogan, "Recognition of Haptic Interaction Patterns in Dyadic Joint Object Manipulation," *IEEE Trans. on Haptics*, vol. 8, pp. 54–66, Jan 2015.

[27] D. J. Agravante, A. Cherubini, A. Bussy, P. Gergondet, and A. Kheddar, "Collaborative Human-Humanoid Carrying Using Vision and Haptic Sensing," in *IEEE Int. Conf. on Robotics and Automation*, 2014.

[28] A. Herdt, H. Diedam, P.-B. Wieber, D. Dimitrov, K. Mombaur, and M. Diehl, "Online walking motion generation with automatic footstep placement," *Advanced Robotics*, vol. 24, no. 5-6, pp. 719–737, 2010.

[29] N. Mansard, O. Stasse, P. Evrard, and A. Kheddar, "A versatile generalized inverted kinematics implementation for collaborative working humanoid robots: The stack of tasks," in *International Conference on Advanced Robotics*, pp. 1–6, IEEE, 2009.

[30] D. J. Agravante, A. Sherikov, P. B. Wieber, A. Cherubini, and A. Kheddar, "Walking pattern generators designed for physical collaboration," in *IEEE Int. Conf. on Robotics and Automation*, 2016.

[31] M. Cutkosky, "On grasp choice, grasp models, and the design of hands for manufacturing tasks," *IEEE Trans. on Robotics and Automation*, vol. 5, pp. 269–279, Jun 1989.

[32] J. Vaillant, A. Kheddar, H. Audren, F. Keith, S. Brossette, A. Escande, K. Bouyarmane, K. Kaneko, M. Morisawa, P. Gergondet, E. Yoshida, S. Kajita, and F. Kanehiro, "Multi-contact vertical ladder climbing with an HRP-2 humanoid," *Autonomous Robots*, vol. 40 (3), pp. 561–580, 2016.

[33] M. Johnson, B. Shrewsbury, S. Bertrand, T. Wu, D. Duran, M. Floyd, P. Abeles, D. Stephen, N. Mertins, A. Lesman, J. Carff, W. Rifenburgh, P. Kaveti, W. Straatman, J. Smith, M. Griffioen, B. Layton, T. de Boer, T. Koolen, P. Neuhaus, and J. Pratt, "Team IHMC's Lessons Learned from the DARPA Robotics Challenge Trials," *Journal of Field Robotics*, vol. 32, no. 2, pp. 192–208, 2015.

[34] S. Feng, E. Whitman, X. Xinjilefu, and C. G. Atkeson, "Optimization-based Full Body Control for the DARPA Robotics Challenge," *Journal of Field Robotics*, vol. 32, no. 2, pp. 293–312, 2015.

[35] A. Herzog, N. Rotella, S. Mason, F. Grimminger, S. Schaal, and L. Righetti, "Momentum control with hierarchical inverse dynamics on a torque-controlled humanoid," *Autonomous Robots*, vol. 40, no. 3, pp. 473–491, 2015.

[36] S. Kuindersma, R. Deits, M. Fallon, A. Valenzuela, H. Dai, F. Permenter, T. Koolen, P. Marion, and R. Tedrake, "Optimization-based locomotion planning, estimation, and control design for the atlas humanoid robot," *Autonomous Robots*, vol. 40, no. 3, pp. 429–455, 2016.

[37] K. Bouyarmane and A. Kheddar, "Using a multi-objective controller to synthesize simulated humanoid robot motion with changing contact configurations," in *IEEE/RSJ Int. Conf. on Intelligent Robots and Systems*, pp. 4414–4419, Sept 2011.

[38] A. Escande, N. Mansard, and P.-B. Wieber, "Hierarchical quadratic programming: Fast online humanoid-robot motion generation," *Int. Journal of Robotics Research*, 2014.

[39] J. Nocedal and S. Wright, *Numerical Optimization*. Springer Series in Operations Research and Financial Engineering, Springer, 2000.

[40] H. Audren, J. Vaillant, A. Kheddar, A. Escande, K. Kaneko, and E. Yoshida, "Model preview control in multi-contact motion-application to a humanoid robot," in *IEEE/RSJ Int. Conf. on Intelligent Robots and Systems*, pp. 4030–4035, Sept 2014.

[41] P.-B. Wieber, R. Tedrake, and S. Kuindersma, "Modeling and control of legged robots," in *Springer handbook of robotics* (B. Siciliano and O. Khatib, eds.), ch. 48, Springer, second ed., 2015.

[42] S. Kajita, F. Kanehiro, K. Kaneko, K. Fujiwara, K. Harada, K. Yokoi, and H. Hirukawa, "Biped walking pattern generation by using preview control of zero-moment point," in *IEEE Int. Conf. on Robotics and Automation*, vol. 2, pp. 1620–1626, 2003.

[43] N. Hogan, "Impedance control - An approach to manipulation. I - Theory. II - Implementation. III - Applications," *ASME Transactions Journal of Dynamic Systems and Measurement Control B*, vol. 107, pp. 1–24, Mar. 1985.

[44] S. Erhart, D. Sieber, and S. Hirche, "An impedance-based control architecture for multi-robot cooperative dual-arm mobile manipulation," in *IEEE/RSJ Int. Conf. on Intelligent Robots and Systems*, 2013.

[45] M. Murooka, S. Nozawa, Y. Kakiuchi, K. Okada, and M. Inaba, "Whole-body pushing manipulation with contact posture planning of large and heavy object for humanoid robot," in *IEEE Int. Conf. on Robotics and Automation*, pp. 5682–5689, May 2015.

[46] W. Chung, L.-C. Fu, and S.-H. Hsu, "Motion Control," in *Springer handbook of robotics* (B. Siciliano and O. Khatib, eds.), ch. 6, pp. 133–159, Springer, 2008.

[47] D. Dimitrov, P.-B. Wieber, H. J. Ferreau, and M. Diehl, "On the implementation of model predictive control for on-line walking pattern generation," in *IEEE Int. Conf. on Robotics and Automation*, 2008.

[48] J. B. Rawlings and D. Q. Mayne, *Model Predictive Control: Theory and Design*. Nob Hill Publishing, 2009.

[49] A. Sherikov, D. Dimitrov, and P.-B. Wieber, "Whole body motion controller with long-term balance constraints," in *IEEE-RAS Int. Conf. on Humanoid Robots*, pp. 444–450, Nov 2014.

[50] N. Bohórquez, A. Sherikov, D. Dimitrov, and P.-B. Wieber, "Safe navigation strategies for a biped robot walking in a crowd," in *IEEE-RAS Int. Conf. on Humanoid Robots*, pp. 379–386, 2016.

[51] A. Sherikov, *Balance preservation and task prioritization in whole body motion control of humanoid robots*. PhD thesis, Communauté Université Grenoble Alpes, Grenoble, France, 2016.

[52] P.-B. Wieber, "Viability and predictive control for safe locomotion," in *IEEE/RSJ Int. Conf. on Intelligent Robots and Systems*, 2008.

[53] P. Zaytsev, S. J. Hasaneini, and A. Ruina, "Two steps is enough: No need to plan far ahead for walking balance," in *IEEE Int. Conf. on Robotics and Automation*, pp. 6295–6300, May 2015.

[54] A. Herdt, N. Perrin, and P.-B. Wieber, "Walking without thinking about it," in *IEEE/RSJ Int. Conf. on Intelligent Robots and Systems*, 2010.

[55] D. J. Agravante, A. Cherubini, A. Bussy, and A. Kheddar, "Human-humanoid joint haptic table carrying task with height stabilization using vision," in *IEEE/RSJ Int. Conf. on Intelligent Robots and Systems*, pp. 4609–4614, 2013.

[56] R. Featherstone, *Rigid body dynamics algorithms*. Springer, 2008.

[57] S. Brossette, A. Escande, G. Duchemin, B. Chrétien, and A. Kheddar, "Humanoid posture generation on non-Euclidean manifolds," in *IEEE-RAS Int. Conf. on Humanoid Robots*, (Seoul, Korea), pp. 352–358, 3-5 November 2015.

[58] A. Rodriguez, M. T. Mason, and S. Ferry, "From caging to grasping," *Int. Journal of Robotics Research*, vol. 31, no. 7, pp. 886–900, 2012.

[59] P. Zaytsev, *Using Controllability of Simple Models to Generate Maximally Robust Walking-Robot Controllers*. PhD thesis, Cornell University, 2015.

[60] O. Stasse, P. Evrard, N. Perrin, N. Mansard, and A. Kheddar, "Fast foot prints re-planning and motion generation during walking in physical human-humanoid interaction," in *humanoids*, pp. 284 – 289, Dec 2009.

[61] D. Serra, C. Brasseur, A. Sherikov, D. Dimitrov, and P.-B. Wieber, "A newton method with always feasible iterates for nonlinear model predictive control of walking in a multi-contact situation," in *IEEE-RAS Int. Conf. on Humanoid Robots*, pp. 932 – 937, 2016.

[62] P. Mittendorfer, E. Yoshida, and G. Cheng, "Realizing whole-body tactile interactions with a self-organizing, multi-modal artificial skin on a humanoid robot," *Advanced Robotics*, vol. 29, no. 1, pp. 51–67, 2015.

[63] C. Brasseur, A. Sherikov, C. Collette, D. Dimitrov, and P.-B. Wieber, "A robust linear MPC approach to online generation of 3D biped walking motion," in *IEEE-RAS Int. Conf. on Humanoid Robots*, 2015.

[64] S. Kajita, M. Morisawa, K. Miura, S. Nakaoka, K. Harada, K. Kaneko, F. Kanehiro, and K. Yokoi, "Biped walking stabilization based on linear inverted pendulum tracking," in *IEEE/RSJ Int. Conf. on Intelligent Robots and Systems*, pp. 4489–4496, Oct 2010.